Energy Storage Properties of Topochemically Synthesized Blue TiO$_2$ Nanostructures in Aqueous and Organic Electrolyte

Parthiban Pazhamalai, Karthikeyan Krishnamoorthy and Sang-Jae Kim

Abstract

This book chapter discusses the topochemical synthesis of blue titanium oxide (b-TiO$_2$) and their application as electrode material for supercapacitor devices in aqueous and organic electrolytes. The formation mechanism of b-TiO$_2$ via topochemical synthesis and their characterization using X-ray diffraction, UV–visible, photoluminescence, electron spin resonance spectroscopy, laser Raman spectrum, X-ray photoelectron spectroscopy, and morphological studies (FESEM and HR-TEM) are discussed in detail. The supercapacitive properties of b-TiO$_2$ electrode were studied using both aqueous (Na$_2$SO$_4$) and organic (TEABF$_4$) electrolytes. The b-TiO$_2$ based symmetric-type supercapacitor (SC) device using TEABF$_4$ works over a wide voltage window (3 V) and delivered a high specific capacitance (3.58 mF cm^{-2}), possess high energy density (3.22 µWh cm^{-2}) and power density (8.06 mW cm^{-2}) with excellent cyclic stability over 10,000 cycles. Collectively, this chapter highlighted the use of b-TiO$_2$ sheets as an advanced electrode for 3.0 V supercapacitors.

Keywords: blue TiO$_2$, topochemical synthesis, electron-spin resonance, photoluminescence, supercapacitors

1. Introduction

The invent of graphene and graphene-like two dimensional materials has created great interest in the exploration of other two-dimensional materials family which includes hexagonal boron nitride, graphitic carbon nitride, transition metal dichalcogenides (TMDCs), layered metal-oxides/double hydroxides, MXenes (transition metal carbides/nitrides), metal–organic frameworks (MOFs), covalent-organic frameworks (COFs), polymers, black phosphorus (BP), siloxene/silicenes, and metallenes [1–7]. In this scenario, the preparation of the 2D materials is of great interest for the development of the new range of materials [8–10]. The preparation methodologies/strategies can be categorized into top-down technique and bottom-up technique [8, 11]. In general, the top-down technique mainly depends on the breakage of the bulk materials to the micro- and nano-scale, whereas in the bottom-up technique, the growth of the materials is from atomic level to the macro-scale

structure [12–14]. Amongst the preparation of the materials, bottom-up techniques such as molecular beam epitaxy, chemical vapor deposition and so on produced high purity and efficient layered materials with desired crystal structure [15–17]. This technique involves in building the nano materials from atomic/molecular scale using heterogeneous/homogeneous chemical reactions, which tend to produce thermodynamically stable materials where the morphology/structure is controlled by both reaction kinetics and thermodynamics [8]. In addition, the building of nanomaterials with desired morphology/structure and composition in a single step is very challenging due to their inherent characteristics of the materials [8, 18]. Moreover, the synthesis of two-dimensional layered materials (metal nitrides/carbides) are hindered due to their non-layered crystal structure. And also, the preparation methods employed in the bottom-up approach is of high cost and the utilization of the prepared materials also requires highly sophisticated instrumentation for characterizing the same. In this regard, top-down technique is of great interest as the cost of production of the materials is less compared to the former with high amount of yield. Some of the top-down approaches for the production of the 2D materials are photolithographic technique, exfoliation (wet and solid phase), mechanical ball milling (wet and solid phase), chemical etching, and topochemical reaction [8, 11]. Amongst the other methods for the top-down technique, topochemical reaction methods is the promising strategy for the preparation of the 2D layered materials [8].

The topochemical route can be classified depends on the reaction methodologies such as adding, extracting or substituting elements to/from the source materials to form the new materials with the retention of the structure/morphology of source material [11]. This type of preparation technique adopts the "corner-overtaking" route, which circumvents the hindrances of direct synthesis through chemical reaction to multi-level steps synthesis [11]. In this aspect, the topochemical preparation route is utilized to synthesize the high value added 2D materials which are difficult to process. Compared to that of the direct synthesis/bottom up approach, top down method has higher advantage to prepare the 2D materials with controlled morphology, composition and material structure. The topochemical reaction route can be performed through various methodologies which includes the (i) selective etching of the elements [19, 20]; (ii) electrochemical methods [21, 22] (iii) high temperature treatment reaction [23, 24] and (iv) liquid phase reaction [25, 26]. In the selective etching methods, the 2D layered materials can be easily obtained by from the bulk counterpart and also it is possible to engineer the interface and surface of the prepared materials. However, the chemical used as etchant is toxic which also affect the quality of the raw materials for the preparation of materials. In this case, hydrofluoric acid is used as the etchant for the preparation of MXenes from the MAX phase element, similarly hydrochloric acid is used for the preparation of siloxene from calcium silicide [27–30]. In case of the electrochemical methods for the preparation, mild and controllable reaction is carried out with the application of electric field to promote the fast reaction [21, 22]. The limitation in this process is that it requires complex instrumentation and the mass production is very limited in the electrochemical method. In the high temperature treatment reaction, the preparation is associated with the controllable atmosphere induced chemical reaction and high temperature condition is employed for the preparation with the limitation of heterogeneity of gas/solid interface reaction, explosion risk at higher temperature and toxic gases as a byproduct of the reaction [23, 24]. Amongst the other techniques in the topochemical reaction, liquid phase exfoliation as the great advantages of high mass yield, wide range of controllable reaction parameters such as solvents, rich experimental/theoretical foundation and produce uniform and good crystalline materials. Hence the liquid phase topochemical methods attains more merits compared to the other methods.

In this book chapter, we have focused on preparing the 2D sheet like blue titanium oxide via liquid phase topochemical reaction on titanium boride. The TiO_2 prepared technique has electron-rich property which shows enormous property in the field of electrochemical energy storage. This electron-rich TiO_2 will be refereed as blue/black TiO_2 which inherits exceptional physical and chemical properties to that of other forms TiO_2 due to their disordered surface structure and Ti^{3+}/oxygen vacancies which leads to high conductivity, magnetic properties, and better chemical properties; yet to be explored for the energy storage application. Herein, the preparation, characterization and the electrochemical properties of blue titanium oxide with sheet-like nanostructures is investigated in detail in this chapter.

2. Preparation of blue titanium oxide (TiO_2) nanosheets

The blue TiO_2 nanosheets was prepared using simple hydrothermal assisted topochemical process as reported in the literature [31, 32]. Initially an appropriate amount of titanium boride was dissolved in 25 mL of hydrofluoric acid and transferred to Teflon lined autoclave for hydrothermal process at 180°C for 12 h. Upon completion of the hydrothermal process, the blue color precipitate is washed with double distilled water/ethanol and dried at 80°C for 12 h to obtain the blue TiO_2 nanosheets.

3. Physicochemical characterization of the blue TiO_2 nanosheets

The blue TiO_2 (blue titanium oxide) nanosheets were prepared using layered TiB_2 and HF as starting materials via hydrothermal process in acidic medium [31]. The mechanism for the formation of layer like blue titanium oxide from the precursor TiB_2 is due to the topochemical reaction as seen in the preparation of siloxenes and MXenes under acidic medium [19, 33]. The TiB_2 is a layered material with titanium and boride arranged in alternating layers. In this case the TiB2 reacts with the HF, which topochemically dissolves boron with the release of hydrogen gas. This generated hydrogen gas creates the oxygen vacancies via H_2 reduction of Ti^{4+} on the surface [31, 34]. The digital micrograph of the precursor and the final product is depicted in the **Figure 1(A)**, which shows the change in from gray TiB_2 to blue colored TiO_2. The X-ray diffraction pattern of the precursor TiB_2 and the prepared TiO_2 were provided in **Figure 1(B)**, which confirms the complete transformation of TiB_2 to TiO_2 and matched with the anatase TiO_2 (JCPDS No: 021-1272) [35]. The implication of the bule colored TiO_2 can be corelated with the vacancy of oxygen, disordered surface and deficiency of oxygen which can be confirmed using the spectroscopic analysis such as electron spin resonance spectroscopy (ESR), UV–visible (UV–vis) and photoluminescence (PL) respectively. The X-band electron spin resonance spectrum of the blue titanium oxide was obtained under the temperature of 77 K with the frequency of 9364 GHz and provided in **Figure 1(C)**. The presence of Ti^{3+} centers in the g- region (ranging from 1.87 to 1.99) which is associated to the resonation of Ti^{3+} species [36]. In addition, the presence of a number of partially overlapping signals in the ESR spectrum is matched well to the different types of Ti^{3+} centers present in the blue titanium oxide. The obtained ESR results is in agreement with the previous finding on the partially reduced TiO_2 [31]. **Figure 1(D)** shows the comparative UV–vis spectra of commercial TiO_2 and blue titanium oxide and the peak observed at 354 nm corresponds to the intrinsic absorption edge of TiO_2 which is red-shifted for the blue titanium oxide to that of the commercial TiO_2 confirming the increase in electron concentration on the surface of blue titanium
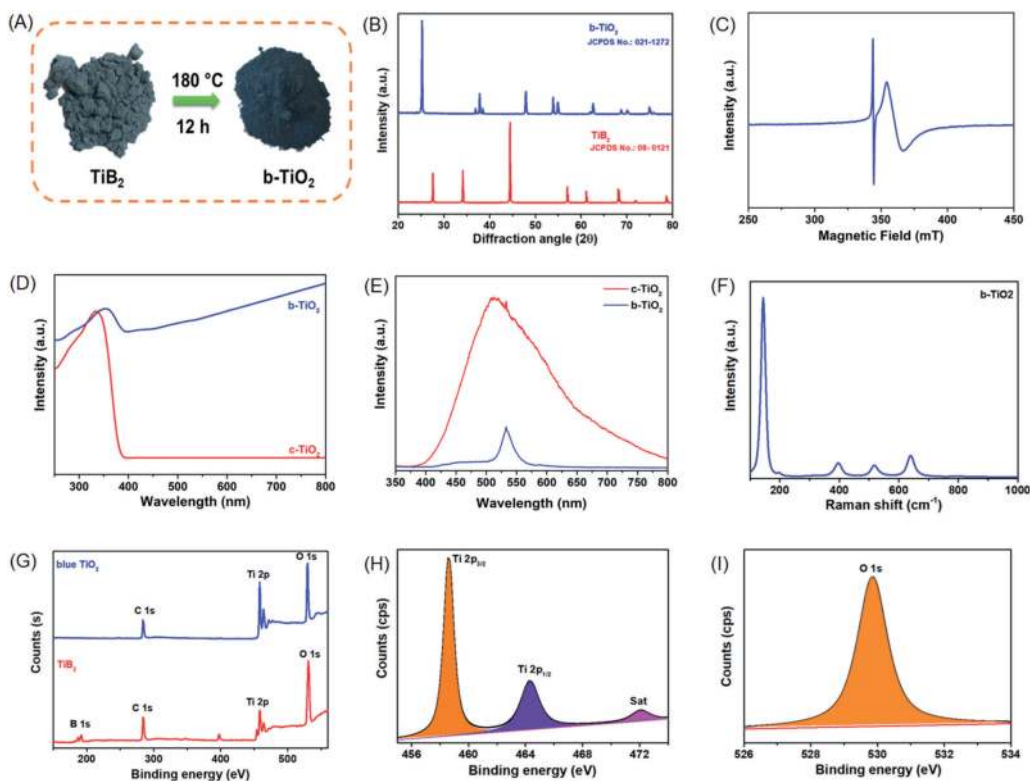
Figure 1.
(A) Digital micrograph of titanium boride and blue titanium oxide. (B) X-ray diffraction pattern of the titanium boride and blue titanium oxide. (C) Electron spin resonance spectrum of blue titanium oxide. (D) UV–visible spectrum of commercial anatase titanium oxide and blue titanium oxide. (E) Photoluminescence spectrum of commercial anatase TiO_2 and blue titanium oxide. (F) Raman spectrum of blue titanium oxide. (G) XPS survey spectrum of TiB_2 and blue titanium oxide. XPS core level spectrum of (H) Ti 2p and (I) O 1 s state in blue titanium oxide.

oxide. Furthermore, the blue titanium oxide shows increased absorbance compared to the commercial TiO_2 over 400–800 nm which is due to the absorbance of low-energy-photon and/or thermal-excitations of trapped electrons in localized states of defects [37–40]. **Figure 1(E)** shows the comparative PL spectra of commercial and prepared TiO_2. The PL spectra depicts the presence of peak over 510–540 nm for the blue titanium oxide compared to that of the commercial TiO_2 which shows a broad band over the region of 400–800 nm [41, 42]. The blue titanium oxide shows higher luminescence intensity to that of the commercial TiO_2 suggesting the low electron–hole recombination rate of blue titanium oxide [43, 44]. These studies confirming the higher electronic conductive states of blue titanium oxide compared to the commercial TiO_2. The laser Raman spectrum of the blue TiO_2 is presented in **Figure 1(F)** which discloses the occurrence of a major vibration band at 148.25 cm^{-1} corresponds to the E_g mode of anatase TiO_2 [45]. In addition to the major vibrational band, the occurrence of the three minor vibrational bands occurred at 396, 517, and 640 cm^{-1} which correspond to the B_{1g}, A_{1g}, and E_g vibrational modes of anatase TiO_2, respectively [38, 46].

The comparative X-ray photoelectron survey spectrum of TiB_2 and blue titanium oxide is provided in **Figure 1(G)**, which shows the presence of Ti 2p, B 1 s, C 1 s and O 1 s states [47]. The existence of oxygen and carbon peaks in the spectrum is due to atmospheric interaction with the sample. From the comparative XPS spectra of TiB_2 and blue titanium oxide, exhibits the complete removal of the boron from TiB_2 which is evident from the XPS spectrum. This study proves the compete dissolution of the boron during the hydrothermal reaction [47]. The XPS spectrum of Ti and O
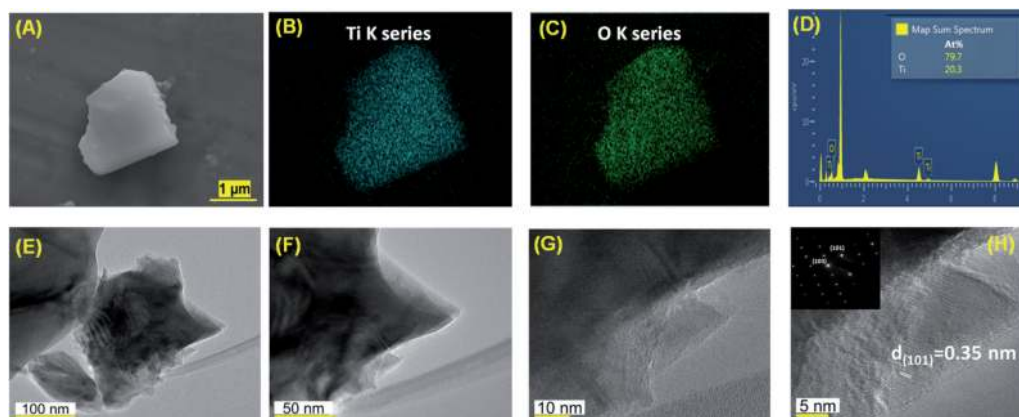
Figure 2.
FESEM and HR-TEM analysis of blue titanium oxide nanostructures.

oxidation states of elements present in the blue titanium oxide nanostructures were provided in **Figure 1(H** and **I)**. The XPS core level spectrum of Ti 2p state reveals the existence of the 2p$_{3/2}$ and 2p$_{1/2}$ at 458, and 464 eV respectively. In addition, the observance of small-satellite peak at 472.2 eV corresponding to the defect of oxygen in the blue titanium oxide [38, 48]. Overall, the core-level spectrum of the titanium highlights the Ti^{4+} oxidation state with littleTi^{3+} state due to oxygen deficiency in blue titanium oxide [49]. **Figure 1(I)** represents the O 1 s states of blue titanium oxide at 530 eV respectively [38, 48]. The calculation of the O/Ti atomic ratio of blue titanium oxide nanostructures is found to be 2.47 from XPS analysis which is in agreement with the literature [50].

To analyze the surface morphology of blue titanium oxide nanostructures field emission scanning electron micrograph (FE-SEM) with energy dispersive spectra (EDS) and high-resolution transmission electron microscope (HR-TEM) were performed. The FE-SEM of blue titanium oxide is provided in **Figure 2(A)**; reveals the presences of nano-sheets/plate-like blue titanium oxide as result of topochemical reaction. The elemental-mapping of Ti & O in the blue titanium oxide is shown in **Figure 2(B** and **C)** and EDS spectrum (**Figure 2(D)**) indicated the homogeneous distributions of Ti and O throughout the blue titanium oxide sheet/plate. With an O/Ti atomic ratio of about 3.92 present in the blue titanium oxide nanostructures [50, 51]. The HR-TEM micrographs of blue titanium oxide obtained under various levels of magnifications are shown in **Figure 2(E–H)**. The HR-TEM micrograph of blue titanium oxide (**Figure 2(E–F)** revealed the presence of sheet-like structures with the lateral size ranging from 200 nm in length and 250 nm in breadth. The magnified portion of **Figure 2(F)** is provided in **Figure 2(G)** reveals the presence of thinner blue titanium oxide sheets with few-layers. The lattice fringes (**Figure 2(H)**) of blue titanium oxide sheets exhibits d = 0.35 nm (an interplanar-spacing) corresponds to (101) plane and SAED pattern (inset of **Figure 2(H)**) reveals the clear diffraction spots signifying the crystallinity-nature of blue titanium oxide [37].

4. Electrochemical characterization of blue titanium oxide electrode

4.1 Preparation of electrode for electrochemical characterization

The working electrode was prepared by mixing the active material (blue titanium oxide) with carbon black and PVDF in an appropriate ratio of 80:15:5 using NMP as solvent. The slurry was spin coated on stainless steel substrate for the three

electrode and two electrode characterizations. For the fabrication of symmetric supercapacitor, CR2032 coin cell configuration is utilized and the TiO_2-coated stainless-steel substrates with an area of 1.86 cm^2 as electrodes separated by a Celgard membrane and 1 M $TEABF_4$ in acetonitrile as the electrolyte. All the electrochemical measurements were performed using an Autolab PGSTAT302N electrochemical workstation.

4.2 Half-cell characterization of blue titanium oxide electrode

The electrochemical properties of the blue titanium oxide electrodes in aqueous electrolyte (half-cell) were inspected using cyclic voltammetry (CV), electrochemical impedance spectroscopy (EIS), and galvanostatic charge–discharge (CD) analysis, respectively. The half-cell electrochemical characterization of the blue titanium oxide electrode was measured in 1 M sodium sulfate electrolyte and provided in **Figure 3**. The cyclic voltammogram provided in **Figure 3(A)** exhibits the existence of the quasi-rectangular behavior suggesting the pseudocapacitive nature of charge-storage in the blue titanium oxide electrode [52, 53]. The indication of the pseudocapacitance nature in blue titanium oxide due to ion-intercalation/de-intercalation phenomenon in addition to the electric double layer/surface capacitance, we quantify the contribution on the overall capacitance using Dunn's method [54]. The plot ofslope of log (i) versus log (ν) obtained from the power law is provided in **Figure 3(B)** [55, 56]:

$$i = a\nu^b \tag{1}$$

where, "ν","a" and "b" are scan rate (mV s^{-1}), adjustable parameters, respectively. The value of "b" is calculated from the slope of log i versus log ν. From the obtained b-value, the nature of the capacitance is evaluated as when b value is 0.5, reveals the diffusion mediated ion-intercalation/de-intercalation whereas the b is 1 represents the surface capacitive nature in the electrode. The contribution of the capacitance related to the surface and diffusion process can be quantified using the relation [54]:

$$I(V) = k_1 \nu + k_2 \nu^{1/2} \tag{2}$$

Were "$k_1 \nu$" and "$k_2 \nu^{1/2}$" related to the contributions from surface- and diffusion-mediated intercalation/de-intercalation process, respectively. The slope and intercept of the plot between $I(V)/v^{1/2}$ and $v^{1/2}$, provides the value of k_1 and k_2 to determine the capacitance contributions [54]. The overall charge stored and their contribution related to the diffusion and surface is calculated using the CV curve in **Figure 3(C)** and the contribution plot is provided in **Figure 3(D)**. From the **Figure 3(D)**, the diffusion capacitance is increasing from 42.10 to 77.29% when the scan rate is decreased from 50 to 5 mV s^{-1}. The diffusion capacitance is higher at the low scan rate which is due to the fact that at high scan rates, the electrolyte ions faces time constraints which limits the diffusion of electrolyte ions whereas low scan rates provide sufficient time for the electrolyte ions to diffuse into the interior surface of the blue titanium oxide electrode [57]. The charge discharge profile shows sloppy symmetric type curves which is evident from **Figure 3(E)** and delivered a high gravimetric specific capacitance of 19 F g-1 and areal capacitance of 19 mF cm^{-2} obtained at a constant current of 0.5 mA as seen in **Figure 3(F)**. The excellent electrochemical performance of the blue titanium oxide in the neutral electrolyte is due to the reason such as sheet-like structure, enhanced electrical conductivity with more oxygen vacant sites in blue titanium oxide.
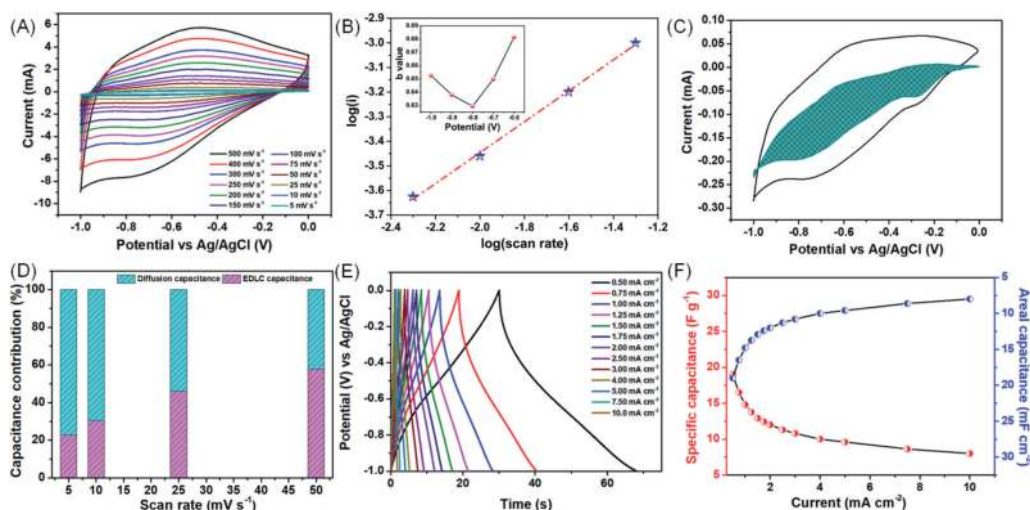
Figure 3.
Three electrode characterization of the blue titanium oxide electrode (A) cyclic voltammetry, (B) plot of log (I) vs. scan rate. The inset in (B) shows the plot of b-values vs. potential. (C) CV profile of blue titanium oxide electrode with the shaded part revealing the capacitive current. (D) Capacitance contribution plot. (E) Galvanostatic charge discharge analysis and the (F) plot of specific capacitance of the blue titanium oxide electrode.

4.3 Full-cell characterization of blue titanium oxide symmetric supercapacitor

In the view point of the practical application, a symmetric supercapacitor is fabricated using blue titanium oxide as electrode and organic liquid (TEABF₄) is used as electrolyte. The electrochemical performance of the fabricated blue titanium oxide SSC was tested for the electrochemical stability of the operating potential window by measuring the CV profiles over the increasing voltage from 0 to 3 3.0 V at a scan rate of 100 mV s^{-1} as shown in **Figure 4**, which shows the distorted rectangular shaped curves and also suggested that the blue titanium oxide SSC device can operate at a window of 3.0 V without any sign of evolution. The cyclic voltammogram of the fabricated SSC displayed typical rectangular shaped curves for all the CV scans at different rates ranging from 5 to 1000 mV s^{-1} (**Figure 5(A** and **B)**) suggesting the pseudocapacitive nature of charge-storage in blue titanium oxide via intercalation/de-intercalation phenomenon [58, 59]. The plot of the scan rate verses specific capacitance is provided in **Figure 5(C)**, depicts a high capacitance of 6.67 F g^{-1} measured at a scan rate of 5 mV s^{-1}. The EIS analysis of the blue titanium oxide SSC is provided in **Figure 5(D–F)** and represented in the form of Nyquist and Bode plots [60]. The high- and mid- frequency region can be used to determine the solution resistance (R_s) or equivalent series resistance (ESR) whereas the low- frequency region directly related to the frequency dependent ion diffusion kinetics of electrolyte ions to the electrode [19]. The values of R_s and R_{ct} from the Nyquist plot are determined to be 1.60 and 15.4 Ω, respectively. The presence of the Warburg element in the model circuit related to the frequency dependent ion diffusion kinetics of electrolyte ions to the electroactive surface as evident from **Figure 5(D)** [61]. **Figure 5(E)** shows the Bode phase angle plot of blue titanium oxide SSCs which tails the phase angle at the low- frequency region (0.01 Hz) is about 64.94°, thus, suggesting the pseudo-capacitive nature of the blue titanium oxide SSCs [33]. **Figure 5(F)** presents the dependence of specific capacitance as a function of applied frequency which is about 3.24 F g^{-1} for the blue titanium oxide SSCs, and the capacitance decreases with respect to an increase in frequency [62].
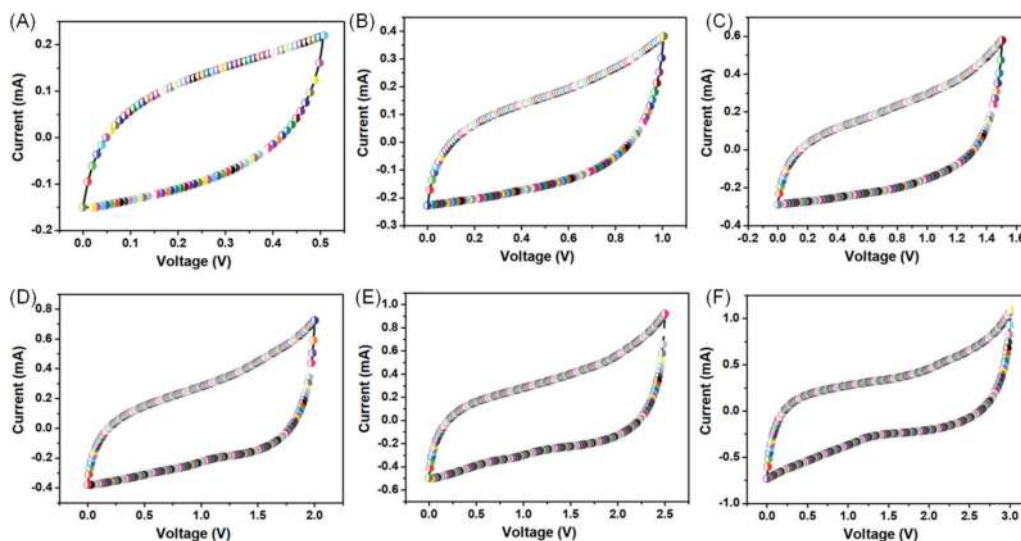
Figure 4.
CV profile ofblue titanium oxide symmetric supercapacitor measured with increasing in voltage window.
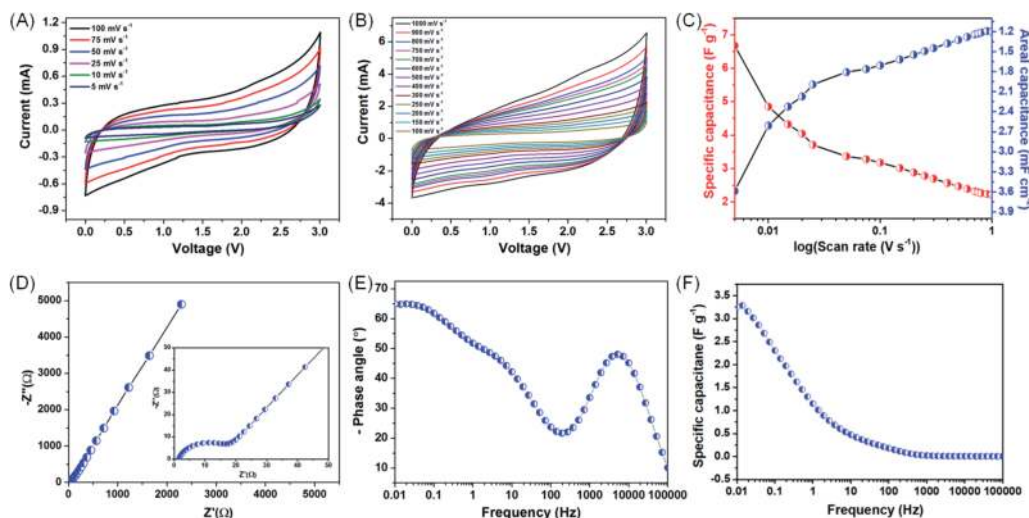

Figure 5.
Full cell characterization of the blue titanium oxide SSC. (A and B) CV profiles and (C) plot of specific capacitance of blue titanium oxide SSC. (D) Nyquist plot and the enlarged portion is provided in the inset; (E) bode phase angle plot and (F) effect of frequency on capacitance blue titanium oxide SSC.

The charge–discharge profiles of the fabricated SSC measured using various constant currents (0.5 to 10 mA) is provided in **Figure 6(A)**. The profiles indicate the existence of the quasi symmetric profiles suggesting the pseudocapacitive behavior of the blue titanium oxide SSCs [63] and the dependance of current on the capacitance is given in **Figure 6(B)**. A high specific capacitance of the 4.80 F g^{-1} is obtained from the GCD profile measured at a constant current of 0.5 mA. The rate capability of the blue titanium oxide SSC device is provided in **Figure 6(C)** which indicating the better capacitance retention when switched from low- to high- current suggesting superior rate capability [19]. The energy and power density plot is represented in the form of Ragone plot (**Figure 6(D)**) which holds a high-energy-density of 6.0 Wh kg^{-1} with a power of about 750 W kg^{-1}, respectively. The long tern cyclic life of the blue titanium oxide SSC depicts the capacitance retention of about 90.2% after 10,000 cycles (**Figure 6(E)**), highlighting the better cycle
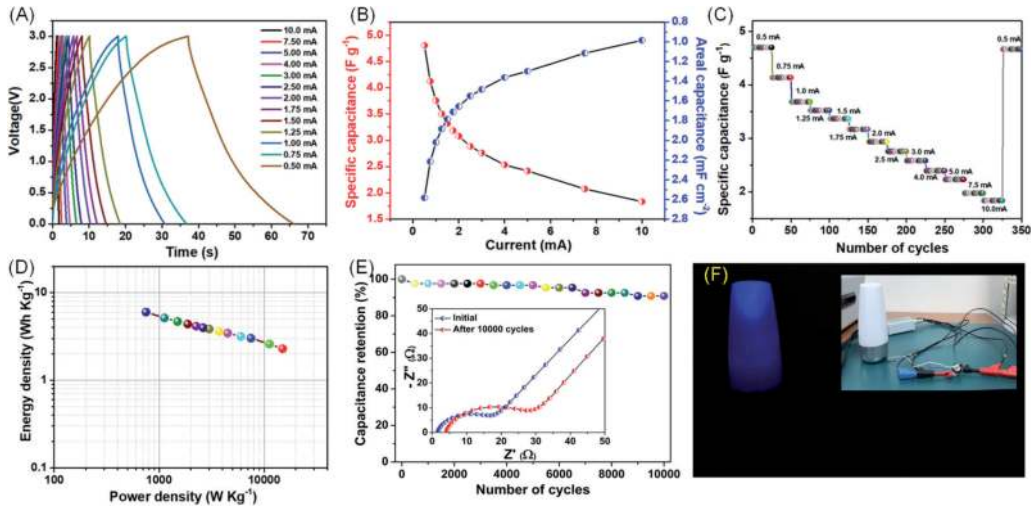
Figure 6.
Full cell characterization of the blue titanium oxide SSC. (A) CD profiles; (B) plot of specific capacitance; (C) rate capability; (D) Ragone plot; (E) cycling stability; the inset in (E) shows the Nyquist plot before and after 10000 cycles of blue titanium oxide SSC device. (F) Real time application of the blue titanium oxide SSC device.

life [25]. The impedance analysis after stability shows the increase in the ESR and charge transfer resistance such as 1.60 to 4.17 Ω and 15.4 to 24.4 Ω. **Figure 6(F)** shows the practical applications of the blue titanium oxide SSC glowing a blue lamp over 10 seconds after charged upto 3 V using a constant current of 0.5 mA.

5. Conclusion

In this book chapter we have demonstrated the preparation of the blue titanium oxide via topochemical reduction of titanium boride in hydrofluoric acid via hydrothermal process. In this we have discussed the formation of 2D layered titanium oxide with oxygen deficiency and the utilization in the energy storage sector. The electrochemical energy storage properties of the blue titanium oxide is tested via symmetric configuration type supercapacitor operated over a wide potential range of 3.0 V with good electrochemical stability and higher rate. The prepared blue titanium oxide shows higher output than those of other 2D electrode materials-based supercapacitors. From overall studies, the prepared materials shows better electrochemical performance which paves the way as a promising electrode material for next-generation smart energy storage sectors.

Acknowledgements

Conflict of interest

"The authors declare no conflict of interest."

Author details

Parthiban Pazhamalai[1], Karthikeyan Krishnamoorthy[1] and Sang-Jae Kim[1,2,3]*

1 Faculty of Applied Energy System, Nanomaterials and System Laboratory, Major of Mechatronics Engineering, Jeju National University, Jeju, Republic of Korea

2 Nanomaterials and System Laboratory, Major of Mechanical System Engineering, College of Engineering, Jeju National University, Jeju, Republic of Korea

3 Research Institute of Energy New Industry, Jeju National University, Jeju, Republic of Korea

*Address all correspondence to: kimsangj@jejunu.ac.kr

IntechOpen

References

[1] Randviir EP, Brownson DAC, Banks CE. A decade of graphene research: Production, applications and outlook. Materials Today. 2014;**17**:426-432. DOI: 10.1016/j.mattod.2014.06.001

[2] Shi Z, Cao R, Khan K, Tareen AK, Liu X, Liang W, et al. Two-dimensional tellurium: Progress, challenges, and prospects. Nano-Micro Letters. 2020;**12**:99. DOI: 10.1007/s40820-020-00427-z

[3] Zeng M, Xiao Y, Liu J, Yang K, Fu L. Exploring two-dimensional materials toward the next-generation circuits: From monomer design to assembly control. Chemical Reviews. 2018;**118**:6236-6296. DOI: 10.1021/acs.chemrev.7b00633

[4] Khan K, Tareen AK, Aslam M, Wang R, Zhang Y, Mahmood A, et al. Recent developments in emerging two-dimensional materials and their applications. Journal of Materials Chemistry C. 2020;**8**:387-440. DOI: 10.1039/C9TC04187G

[5] Forouzandeh P, Pillai SC. Two-dimensional (2D) electrode materials for supercapacitors. Materials Today: Proceedings. 2021;**41**:498-505. DOI: 10.1016/j.matpr.2020.05.233

[6] Pham VP. Direct growth of graphene on flexible substrates toward flexible electronics: A promising perspective. In: Flex. Electron. InTech; 2018. DOI: 10.5772/intechopen.73171

[7] Pham VP, Yeom GY. Recent advances in doping of molybdenum disulfide: Industrial applications and future prospects. Advanced Materials. 2016;**28**:9024-9059. DOI: 10.1002/adma.201506402

[8] Zhang Q, Peng W, Li Y, Zhang F, Fan X. Topochemical synthesis of low-dimensional nanomaterials.

Nanoscale. 2020;**12**:21971-21987. DOI: 10.1039/D0NR04763E

[9] Pazhamalai P, Krishnamoorthy K, Mariappan VK, Sathyaseelan A, Kim S-J. Solar driven renewable energy storage using rhenium disulfide nanostructure based rechargeable supercapacitors. Materials Chemistry Frontiers. 2020;**4**:3290-3301. DOI: 10.1039/D0QM00421A

[10] Pazhamalai P, Krishnamoorthy K, Mariappan VK, Sahoo S, Manoharan S, Kim S-J. A high efficacy self-charging MoSe₂ solid-state supercapacitor using electrospun nanofibrous piezoelectric separator with ionogel electrolyte. Advanced Materials Interfaces. 2018;**5**:1800055. DOI: 10.1002/admi.201800055

[11] Xiao X, Wang H, Urbankowski P, Gogotsi Y. Topochemical synthesis of 2D materials. Chemical Society Reviews. 2018;**47**:8744-8765. DOI: 10.1039/C8CS00649K

[12] Gopalakrishnan D, Damien D, Shaijumon MM. MoS₂ quantum dot-interspersed exfoliated MoS₂ nanosheets. ACS Nano. 2014;**8**:5297-5303. DOI: 10.1021/nn501479e

[13] Saha SK, Baskey M, Majumdar D. Graphene quantum sheets: A new material for spintronic applications. Advanced Materials. 2010;**22**:5531-5536. DOI: 10.1002/adma.201003300

[14] Chhowalla M, Shin HS, Eda G, Li L-J, Loh KP, Zhang H. The chemistry of two-dimensional layered transition metal dichalcogenide nanosheets. Nature Chemistry. 2013;**5**:263-275. DOI: 10.1038/nchem.1589

[15] Li S, Lin YC, Zhao W, Wu J, Wang Z, Hu Z, et al. Vapour-liquid-solid growth of monolayer MoS₂ nanoribbons. Nature Materials. 2018;**17**:535-542. DOI: 10.1038/s41563-018-0055-z

[16] Zhao X, Ning S, Fu W, Pennycook SJ, Loh KP. Differentiating polymorphs in molybdenum disulfide via electron microscopy. Advanced Materials. 2018;**30**:1-11. DOI: 10.1002/adma.201802397

[17] Ares P, Palacios JJ, Abellán G, Gómez-Herrero J, Zamora F. Recent progress on antimonene: A new bidimensional material. Advanced Materials. 2018;**30**:1703771. DOI: 10.1002/adma.201703771

[18] Mizuguchi R, Imai H, Oaki Y. Formation processes, size changes, and properties of nanosheets derived from exfoliation of soft layered inorganic–organic composites. Nanoscale Advances. 2020;**2**:1168-1176. DOI: 10.1039/D0NA00084A

[19] Krishnamoorthy K, Pazhamalai P, Kim S-JJ. Two-dimensional siloxene nanosheets: Novel high-performance supercapacitor electrode materials. Energy & Environmental Science. 2018;**11**:1595-1602. DOI: 10.1039/C8EE00160J

[20] Pazhamalai P, Krishnamoorthy K, Sahoo S, Mariappan VK, Kim SJ. Understanding the thermal treatment effect of two-dimensional siloxene sheets and the origin of superior electrochemical energy storage performances. ACS Applied Materials & Interfaces. 2019;**11**:624-633. DOI: 10.1021/acsami.8b15323

[21] Ambrosi A, Pumera M. Exfoliation of layered materials using electrochemistry. Chemical Society Reviews. 2018;**47**:7213-7224. DOI: 10.1039/C7CS00811B

[22] Yang S, Zhang P, Nia AS, Feng X. Emerging 2D materials produced via electrochemistry. Advanced Materials. 2020;**32**:1907857. DOI: 10.1002/adma.201907857

[23] Jeon J, Park Y, Choi S, Lee J, Lim SS, Lee BH, et al. Epitaxial synthesis of molybdenum carbide and formation of a Mo_2 C/MoS_2 hybrid structure via chemical conversion of molybdenum disulfide. ACS Nano. 2018;**12**:338-346. DOI: 10.1021/acsnano.7b06417

[24] Cao J, Li T, Gao H, Lin Y, Wang X, Wang H, et al. Realization of 2D crystalline metal nitrides via selective atomic substitution. Science Advances. 2020;**6**. DOI: 10.1126/sciadv.aax8784

[25] Li H, Jing L, Liu W, Lin J, Tay RY, Tsang SH, et al. Scalable production of few-layer boron sheets by liquid-phase exfoliation and their superior supercapacitive performance. ACS Nano. 2018;**12**:1262-1272. DOI: 10.1021/acsnano.7b07444

[26] Shen J, He Y, Wu J, Gao C, Keyshar K, Zhang X, et al. Liquid Phase Exfoliation of Two-Dimensional Materials by Directly Probing and Matching Surface Tension Components. Nano Letters. 2015;**15**:5449-5454. DOI: 10.1021/acs.nanolett.5b01842

[27] Navarro-Suárez AM, Van Aken KL, Mathis T, Makaryan T, Yan J, Carretero-González J, et al. Development of asymmetric supercapacitors with titanium carbide-reduced graphene oxide couples as electrodes. Electrochimica Acta. 2018;**259**:752-761. DOI: 10.1016/j.electacta.2017.10.125

[28] Wang F, Wu X, Yuan X, Liu Z, Zhang Y, Fu L, et al. Latest advances in supercapacitors: From new electrode materials to novel device designs. Chemical Society Reviews. 2017;**46**:6816-6854. DOI: 10.1039/c7cs00205j

[29] Nakano H, Ohtani O, Mitsuoka T, Akimoto Y, Nakamura H. Synthesis of amorphous silica nanosheets and their photoluminescence. Journal of the American Ceramic Society. 2005;**88**:3522-3524. DOI: 10.1111/j.1551-2916.2005.00618.x

[30] Ramachandran R, Leng X, Zhao C, Xu Z-X, Wang F. 2D siloxene sheets: A novel electrochemical sensor for selective dopamine detection. Applied Materials Today. 2020;**18**:100477. DOI: 10.1016/j.apmt.2019.100477

[31] Chiesa M, Livraghi S, Giamello E, Albanese E, Pacchioni G. Ferromagnetic Interactions in Highly Stable, Partially Reduced TiO2: The S=2 State in Anatase. Angewandte Chemie. 2017;**56**:2604-2607. DOI: 10.1002/anie.201610973

[32] Pazhamalai P, Krishnamoorthy K, Mariappan VK, Kim S-JJ. Blue TiO2 nanosheets as a high-performance electrode material for supercapacitors. Journal of Colloid and Interface Science. 2019;**536**:62-70. DOI: 10.1016/j.jcis.2018.10.031

[33] Krishnamoorthy K, Pazhamalai P, Sahoo S, Kim SJ. Titanium carbide sheet based high performance wire type solid state supercapacitors. Journal of Materials Chemistry A. 2017;**5**:5726-5736. DOI: 10.1039/C6TA11198J

[34] C.Z. Wen, H.B. Jiang, S.Z. Qiao, H.G. Yang, G.Q. (Max) Lu, Synthesis of high-reactive facets dominated anatase TiO2, Journal of Materials Chemistry 21 (2011) 7052. doi:10.1039/c1jm00068c.

[35] Righini L, Gao F, Lietti L, Szanyi J, Peden CHF. Performance and properties of K and TiO2 based LNT catalysts. Applied Catalysis B: Environmental. 2016;**181**:862-873. DOI: 10.1016/j.apcatb.2015.07.008

[36] Chiesa M, Paganini MC, Livraghi S, Giamello E. Charge trapping in TiO2 polymorphs as seen by Electron Paramagnetic Resonance spectroscopy. Physical Chemistry Chemical Physics. 2013;**15**:9435. DOI: 10.1039/c3cp50658d

[37] Zhu Q, Peng Y, Lin L, Fan C-M, Gao G-Q, Wang R-X, et al. Stable blue TiO2−x nanoparticles for efficient visible light photocatalysts. Journal of Materials Chemistry A. 2014;**2**:4429. DOI: 10.1039/c3ta14484d

[38] Liu G, Yang HG, Wang X, Cheng L, Lu H, Wang L, et al. Enhanced photoactivity of oxygen-deficient anatase TiO2 sheets with dominant {001} facets. Journal of Physical Chemistry C. 2009;**113**:21784-21788. DOI: 10.1021/jp907749r

[39] Qiu J, Li S, Gray E, Liu H, Gu Q-F, Sun C, et al. Hydrogenation Synthesis of Blue TiO2 for High-Performance Lithium-Ion Batteries. Journal of Physical Chemistry C. 2014;**118**:8824-8830. DOI: 10.1021/jp501819p

[40] Dong J, Han J, Liu Y, Nakajima A, Matsushita S, Wei S, et al. Defective black TiO2 synthesized via anodization for visible-light photocatalysis. ACS Applied Materials & Interfaces. 2014;**6**:1385-1388. DOI: 10.1021/am405549p

[41] Zhang C, Hua H, Liu J, Han X, Liu Q, Wei Z, et al. Enhanced Photocatalytic Activity of Nanoparticle-Aggregated Ag–AgX(X = Cl, Br)@TiO2 Microspheres Under Visible Light. Nano-Micro Letters. 2017;**9**:49. DOI: 10.1007/s40820-017-0150-8

[42] Knorr FJ, Mercado CC, McHale JL. Trap-State Distributions and Carrier Transport in Pure and Mixed-Phase TiO 2 : Influence of Contacting Solvent and Interphasial Electron Transfer. Journal of Physical Chemistry C. 2008; **112**:12786-12794. DOI: 10.1021/jp8039934

[43] Jiang Z, Wan W, Wei W, Chen K, Li H, Wong PK, et al. Gentle way to build reduced titanium dioxide nanodots integrated with graphite-like carbon spheres: From DFT calculation to experimental measurement. Applied Catalysis B: Environmental. 2017;**204**:283-295. DOI: 10.1016/j.apcatb.2016.11.044

[44] Jin C, Liu B, Lei Z, Sun J. Structure and photoluminescence of the TiO2 films grown by atomic layer deposition using tetrakis-dimethylamino titanium and ozone. Nanoscale Research Letters. 2015;**10**:95. DOI: 10.1186/s11671-015-0790-x

[45] Yan J, Wu G, Guan N, Li L, Li Z, Cao X. Understanding the effect of surface/bulk defects on the photocatalytic activity of TiO2: Anatase versus rutile. Physical Chemistry Chemical Physics. 2013;**15**:10978-10988. DOI: 10.1039/c3cp50927c

[46] Ohsaka T, Izumi F, Fujiki Y. Raman spectrum of anatase, TiO2. Journal of Raman Specroscopy. 1978;**7**:321-324. DOI: 10.1002/jrs.1250070606

[47] Li L, Qiu F, Wang Y, Wang Y, Liu G, Yan C, et al. Crystalline TiB 2: An efficient catalyst for synthesis and hydrogen desorption/absorption performances of NaAlH 4 system. Journal of Materials Chemistry. 2012;**22**:3127-3132. DOI: 10.1039/c1jm14936a

[48] Erdem B, Hunsicker RA, Simmons GW, David Sudol E, Dimonie VL, El-Aasser MS. XPS and FTIR surface characterization of TiO2 particles used in polymer encapsulation. Langmuir. 2001;**17**:2664-2669. DOI: 10.1021/la0015213

[49] Bapna K, Phase DM, Choudhary RJ. Study of valence band structure of Fe doped anatase TiO 2 thin films. Journal of Applied Physics. 2011;**110**:043910. DOI: 10.1063/1.3624775

[50] Lin T, Yang C, Wang Z, Yin H, Lü X, Huang F, et al. Effective nonmetal incorporation in black titania with enhanced solar energy utilization. Energy & Environmental Science. 2014;**7**:967. DOI: 10.1039/c3ee42708k

[51] Kong L, Jiang Z, Wang C, Wan F, Li Y, Wu L, et al. Simple Ethanol

Impregnation Treatment Can Enhance Photocatalytic Activity of TiO 2 Nanoparticles under Visible-Light Irradiation. ACS Applied Materials & Interfaces. 2015;**7**:7752-7758. DOI: 10.1021/acsami.5b00888

[52] Xia Y, Mathis TS, Zhao MQ, Anasori B, Dang A, Zhou Z, et al. Thickness-independent capacitance of vertically aligned liquid-crystalline MXenes. Nature. 2018;**557**:409-412. DOI: 10.1038/s41586-018-0109-z

[53] Lukatskaya MR, Kota S, Lin Z, Zhao M-QQ, Shpigel N, Levi MD, et al. Ultra-high-rate pseudocapacitive energy storage in two-dimensional transition metal carbides. Nature Energy. 2017;**2**:17105. DOI: 10.1038/nenergy.2017.105

[54] Wang J, Polleux J, Lim J, Dunn B. Pseudocapacitive contributions to electrochemical energy storage in TiO 2 (anatase) nanoparticles. Journal of Physical Chemistry C. 2007;**111**:14925-14931. DOI: 10.1021/jp074464w

[55] Jiang Q, Kurra N, Alhabeb M, Gogotsi Y, Alshareef HN. All Pseudocapacitive MXene-RuO2 Asymmetric Supercapacitors. Advanced Energy Materials. 2018;**8**:1703043. DOI: 10.1002/aenm.201703043

[56] Mariappan VK, Krishnamoorthy K, Pazhamalai P, Sahoo S, Kim SJ. Electrodeposited molybdenum selenide sheets on nickel foam as a binder-free electrode for supercapacitor application. Electrochimica Acta. 2018;**265**:514-522. DOI: 10.1016/j.electacta.2018.01.075

[57] Huang B, Wang W, Pu T, Li J, Zhu J, Zhao C, et al. Two-dimensional porous (Co, Ni)-based monometallic hydroxides and bimetallic layered double hydroxides thin sheets with honeycomb-like nanostructure as positive electrode for high-performance hybrid supercapacitors. Journal of Colloid and Interface Science.

2018;**532**:630-640. DOI: 10.1016/j.jcis.2018.08.019

[58] Han J, Hirata A, Du J, Ito Y, Fujita T, Kohara S, et al. Intercalation pseudocapacitance of amorphous titanium dioxide@nanoporous graphene for high-rate and large-capacity energy storage. Nano Energy. 2018;**49**:354-362. DOI: 10.1016/j.nanoen.2018.04.063

[59] Wang J, Polleux J, Brezesinski T, Tolbert S, Dunn B. The Pseudocapacitance Behaviors of TiO2 (Anatase) Nanoparticles. ECS Transactions. 2008:101-111. DOI: 10.1149/1.2953511

[60] Fong KD, Wang T, Kim HK, Kumar RV, Smoukov SK. Semi-Interpenetrating Polymer Networks for Enhanced Supercapacitor Electrodes. ACS Energy Letters. 2017;**2**:2014-2020. DOI: 10.1021/acsenergylett.7b00466

[61] Sahoo S, Pazhamalai P, Krishnamoorthy K, Kim SJ. Hydrothermally prepared α-MnSe nanoparticles as a new pseudocapacitive electrode material for supercapacitor. Electrochimica Acta. 2018;**268**:403-410. DOI: 10.1016/j.electacta.2018.02.116

[62] Rakhi RB, Ahmed B, Hedhili MN, Anjum DH, Alshareef HN. Effect of Postetch Annealing Gas Composition on the Structural and Electrochemical Properties of Ti2CTx MXene Electrodes for Supercapacitor Applications. Chemistry of Materials. 2015;**27**:5314-5323. DOI: 10.1021/acs.chemmater.5b01623

[63] Barai HR, Rahman MM, Joo SW. Template-free synthesis of two-dimensional titania/titanate nanosheets as electrodes for high-performance supercapacitor applications. Journal of Power Sources. 2017;**372**:227-234. DOI: 10.1016/j.jpowsour.2017.10.076